IEEE Access
Multidisciplinary : Rapid Review : Open Access Journal

Received March 20, 2022, accepted April 7, 2022, date of publication April 11, 2022, date of current version April 26, 2022.

Digital Object Identifier 10.1109/ACCESS.2022.3166464

Compressive Sampling of Color Retinal Image Using Spread Spectrum Fourier Sampling and Total Variant

LEDYA NOVAMIZANTI[1], (Student Member, IEEE), I NYOMAN APRAZ RAMATRYANA[2], (Student Member, IEEE), RITA MAGDALENA[1], I PUTU AGUS EKA PRATAMA[3], TARIQ RAHIM[4], (Member, IEEE), AND SOO YOUNG SHIN[2], (Senior Member, IEEE)

[1]School of Electrical Engineering and Human Centric Engineering, Telkom University, Bandung 40257, Indonesia
[2]Department of IT Convergence Engineering, Kumoh National Institute of Technology, Gumi 39177, Republic of Korea
[3]Department of Information Technology, Faculty of Engineering, Udayana University, Bukit Jimbaran, Bali 80361, Indonesia
[4]Cardiff School of Health and Sciences, Cardiff Metropolitan University, Cardiff CF5 2YB, U.K.

Corresponding author: Ledya Novamizanti (ledyaldn@telkomuniversity.ac.id)

This work was supported in part by the Directorate of Research and Community Service, Telkom University, and in part by the Indonesian Endowment Fund for Education (LPDP) Scholarships.

ABSTRACT In medical imaging, the application of retinal images demands a lot of retinal photos to analyze and requires efficient compression techniques for retinal image storage. Retinal images must meet stringent quality requirements for clinical data to be accurate and dependable. This paper proposes a compressive sampling (CS) framework for color retinal image (CRI) compression, which relies on spread spectrum Fourier sampling (SSFS) and total variant (TV)-based reconstruction method with three loops of RGB color space, referred to as RGB-TV. In CS, two procedures are performed, i.e., compression and CS reconstruction. In compression steps, SFFS is performed to get a compressed signal from the original CRI with a high compression ratio (CR). While in CS reconstruction, TV-norm and TV proximal operator are exploited for problem optimization to recover original CRI from a compressed signal. In addition, signal-to-noise ratio (SNR), structural similarity (SSIM), and reconstruction time are investigated for the performance metrics of the proposed RGB-TV. The computer simulation result shows that the proposed RGB-TV with a set of CRI of size 512 by 512 pixels can compress until CR = 10 which obtains mean SNR of 22 dB, SSIM 0.84, and reconstruction time of 2.2 seconds.

INDEX TERMS Color retinal image, compressive sampling, RGB, spread spectrum, total variant.

I. INTRODUCTION

For many years, the application of retinal image in medical imaging was studied by researchers, i.e., automatic cataract classification [1], diabetic retinopathy [2], cholesterol level detection [3]–[5], automatic vessel segmentation [6], and retinal prosthesis [7]. These applications demand a lot of retinal images to analyze and require efficient compression techniques for retinal image storage. In addition, because monitoring such retinal images is a complex undertaking, retinal images must meet stringent quality requirements in order for clinical data to be accurate and dependable. This challenge can be mitigated with the use of effective retinal image compression algorithms [8].

The associate editor coordinating the review of this manuscript and approving it for publication was Gang Wang.

In medical image compression (MIC), various lossy and lossless compression framework were developed. The lossless MICs were proposed, such as a segmentation-based lossless image coding [9], wavelet-based compression scheme [10], adaptive predictive multiplicative autoregressive [11], advanced video coding scheme (H.264/AVC) [12], symmetry-based technique for scalable lossless compression [13], minimum rate predictors [14], and end-to-end optimized learning framework with intra-slice and inter-slice redundancy [15]. In addition, the lossy MICs were developed, i.e., a wavelet-based compression using distortion-constrained adaptive vector quantization [16], optimized volume of interest coding [17], high efficiency video coding [18], and lossy-to-lossless data compression scheme [19]. Moreover, this paper considers a compression framework based on compressive sensing for medical images.

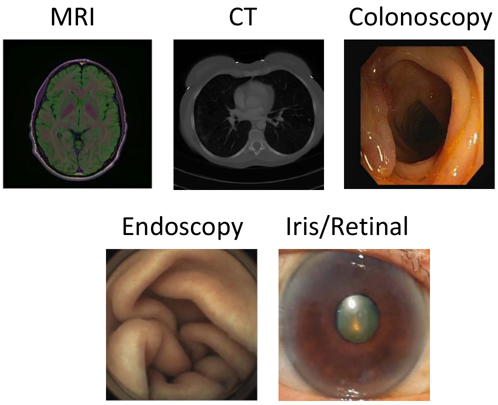

FIGURE 1. An example of medical imaging.

Compressive sampling (CS) was proposed as an approach to sampling a sparse signal with number of sample is less than the Nyquist theorem and the sampled signal can be recovered using a reconstruction method [20]–[22]. Many CS applications in different fields were developed, such as geoscience and remote sensing [23], antennas and wireless propagation [24], signal processing [25], intelligent transportation systems [26], wireless communications [27], and watermarking systems [28], [29]. However, in medical imaging, CS is exploited to speedup the medical investigation time [30].

Recently, an application of CS for MIC using multiple dictionaries of sparse basis was proposed, called compressed medical imaging (CMI) using multi-basis reweighted analysis (M-BRA) [31]. CMI reduces the operational time of medical devices with a sparse acquisition process and stores the samples in the CS domain. This benefit gives less processing time to a patient from medical devices [32]. The transmission, storage, and representation issues in a smaller size with a high perceived quality can also be improved. In [31], four types of medical imaging are considered, i.e., computed tomography, wireless capsule endoscopy images, colonoscopy images, and magnetic resonance imaging. Reference [31] only considers the grayscale format as the input of the proposed CMI. However, color medical images are quite sensitive, need a good quality medical analysis in color feature, and require a CMI in color space (RGB format). Fig. 1 shows an example of medical imaging where colonoscopy, endoscopy, and iris/retinal images are color medical imaging. An initial CMI framework in color medical images considering RGB format was proposed using sparsity averaging (SA) reweighted analysis (RA) and referred to as RGB-SARA [33]. In addition, the CMI of color iris/retinal images using basis pursuit (BP) with SA (RGB-BPSA) [34] was proposed. The previous RGB-based CMI was mostly based on BP where ℓ_1 normalization is exploited for CS reconstruction. To the best of the author's knowledge, total variant (TV)-based CMI for a color medical image is not proposed and investigated yet.

Throughout this paper, a novel TV-based reconstruction method for RGB color retinal images (RGB-TV) is proposed. Different from RGB-SARA [33] and M-BRA [31], RA is not considered in this paper because RA process requires long processing time. This paper aims to reduce the time process and improve the visual quality of CMI. Furthermore, this article presents the CMI contributions as follows

- Novel MIC for a color retinal image is proposed by exploiting CMI to achieve high CR in MIC.
- Novel RGB-based CMI using spread spectrum (SS) Fourier sampling and TV regularization.
- Performance improvement using TV-based CMI and comparison of TV and BP regularization for CS reconstruction.

The rest of this paper is organized as follows. Section II briefly describes the related works. Section III presents CS for compression. In Section IV, the proposed RGB-TV is introduced in detail. Section V presents retinal images, performance metrics, and experiment scenarios. Experiment results are shown in Section VI. Last, Section VII describes the conclusion of this paper.

II. RELATED WORKS

The previous CS framework was proposed using a wavelet-based sparsity basis [20]. Then, a new sparsity basis approach was proposed using the average of multiple sparsity basis prior for radio astronomy images and referred to as sparsity averaging reweighted analysis (SARA) [35]. In addition, an enhanced SARA was proposed by exploiting double concatenated of SARA basis and BP regularization in CS reconstruction of medical imaging, called DC-SARA [36]. Next, a generalized version of DC-SARA was proposed and referred to as M-BRA [31]. However, SARA, DC-SARA, and M-BRA exploit BP for CS reconstruction, while a SARA based on TV was proposed to speedup the reconstruction time of SARA [37]. Last, MIC for the retinal images was proposed by using CS framework based on BP and average sparsity model [34].

III. CS FOR COMPRESSION

In this article, the sparse signal and the compressed signal are denoted by $\boldsymbol{x}$ and $\boldsymbol{y}$, respectively. Fig. 2 shows the illustration of CS, i.e., compression and CS reconstruction for color retinal image (CRI).

A. COMPRESSION

In compression, a signal $\boldsymbol{x} \in \mathbb{C}^{n\times 1}$ is sampled by a sensing matrix $\boldsymbol{\Phi} \in \mathbb{C}^{m\times n}$ to get a compressed signal $\boldsymbol{y} \in \mathbb{C}^{m\times 1}$ with less m-number of samples. The compression process in CS is defined as

$$\boldsymbol{y} = \boldsymbol{\Phi x}. \tag{1}$$

Suppose an CRI is represented by two-dimensional signal $\boldsymbol{I}$, then $\boldsymbol{I}$ is reshaped to one-dimensional signal $\boldsymbol{s} \in \mathbb{R}^{n\times 1}$. The requirement of CS as follows, first, if $\boldsymbol{s}$ is sparse, then $\boldsymbol{x} = \boldsymbol{s}$,

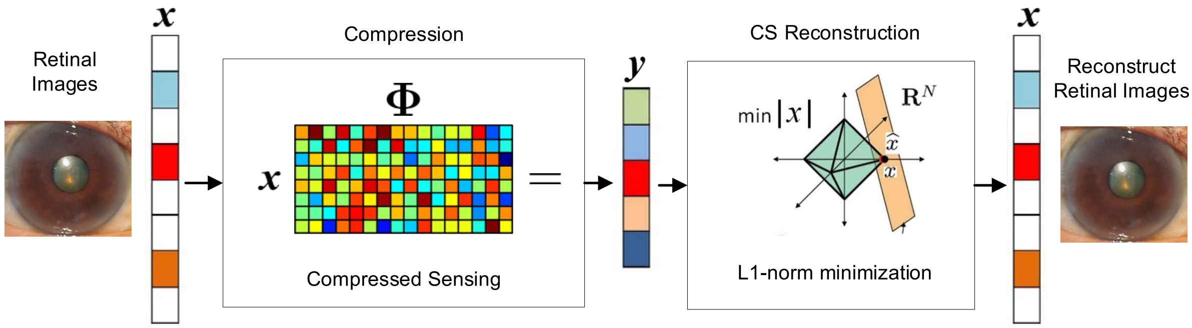

FIGURE 2. An illustration of MIC framework that exploit CS for CRI.

while if $\boldsymbol{s}$ is not sparse, then $\boldsymbol{s}$ is transformed by sparsity basis Ψ to a sparse signal $\boldsymbol{x}$ or $\boldsymbol{x} = \boldsymbol{\Psi s}$. The compression becomes

$$\boldsymbol{y} = \boldsymbol{\Phi \Psi s}, \tag{2}$$

where $\boldsymbol{\Psi} \in \mathbb{C}^{n \times n}$ represents the sparsity basis, $\boldsymbol{s} \in \mathbb{C}^{n \times 1}$ represent the signal, and $\boldsymbol{\Phi}$ represents the compression matrix.

B. CS RECONSTRUCTION

In CS reconstruction, a signal reconstructed signal $\hat{\boldsymbol{x}}$ is recovered from $\boldsymbol{y}$ and known $\boldsymbol{\Phi}$ and the reconstruction process can be modeled by a convex problem as

$$\min_{\hat{\boldsymbol{x}}} \left\|\hat{\boldsymbol{x}}\right\|_1 \quad \text{s. t. } \|\boldsymbol{y} - \boldsymbol{\Phi}\hat{\boldsymbol{x}}\|_2 \leq \varepsilon, \tag{3}$$

where $\hat{\boldsymbol{x}}$, $\|\cdot\|_2$, ℓ_2 norm, ε, and $\|\cdot\|_1$ represent the reconstructed sparse signal, ℓ_2 norm upper bound, and ℓ_1 norm. From Eq. (1), suppose $\boldsymbol{\Phi}$, $\boldsymbol{\Psi}$, and $\boldsymbol{y}$ are known, then the optimization problem becomes

$$\hat{s} = \min_{s} \|s\|_1 \quad \text{s. t. } \|\boldsymbol{y} - \boldsymbol{\Phi \Psi}\hat{s}\|_2 \leq \varepsilon. \tag{4}$$

Furthermore, $\hat{I}$ denotes the reconstructed CRI.

C. CS PERFORMANCE METRICS

In CS, compression ratio (CR) is the ratio of $\boldsymbol{x}$ and $\boldsymbol{y}$ as shown in Fig. 2 and defined as

$$\text{CR} = \frac{n}{m}, \tag{5}$$

with n and m are the dimension size of $\boldsymbol{\Phi}$.

The signal to noise ratio (SNR) is calculated from an original image $\boldsymbol{s}$ and a result image $\hat{\boldsymbol{s}}$ and determined as

$$\text{SNR} = \frac{1}{3}\sum_{l=1}^{3} 10\log_{10}\left(\frac{\|s_l\|_2}{\left\|s_l - \hat{s}_l\right\|_2}\right)^2, \tag{6}$$

where l is each color layer of RGB.

The structural similarity (SSIM) is a perceptual metric that represents the loss of quality in data compression based on contrast, luminance, and structure of the image which are defined as follows

$$\text{con}(\boldsymbol{s}, \hat{\boldsymbol{s}}) = \frac{2\sigma_s\sigma_{\hat{s}} + \text{C}_2}{\sigma_s^2 + \sigma_{\hat{s}}^2 + \text{C}_2},$$

$$\text{lum}(\boldsymbol{s}, \hat{\boldsymbol{s}}) = \frac{2\mu_s\mu_{\hat{s}} + \text{C}_1}{\mu_s^2 + \mu_{\hat{s}}^2 + \text{C}_1},$$

$$\text{struc}(\boldsymbol{s}, \hat{\boldsymbol{s}}) = \frac{\sigma_{s\hat{s}} + \text{C}_3}{\sigma_s\sigma_{\hat{s}} + \text{C}_3}, \tag{7}$$

where σ_s and μ_s denote local standard deviation and mean of the pixel in original CRI. $\sigma_{\hat{s}}$ and $\mu_{\hat{s}}$ denote local standard deviation and mean of the pixel in result image. $\sigma_{s\hat{s}}$ denotes cross-covariance between $\boldsymbol{s}$ and $\hat{\boldsymbol{s}}$. Next, SSIM defined as

$$\text{SSIM}(\boldsymbol{s}, \hat{\boldsymbol{s}}) = [\text{con}(\boldsymbol{s}, \hat{\boldsymbol{s}})]^{\beta} \cdot [\text{lum}(\boldsymbol{s}, \hat{\boldsymbol{s}})]^{\alpha} \cdot [\text{struc}(\boldsymbol{s}, \hat{\boldsymbol{s}})]^{\gamma}. \tag{8}$$

Let C_3, $\text{C}_3 = \frac{\text{C}_2}{2}$, and $\alpha = \beta = \gamma = 1$ are assumed as default, SSIM becomes

$$\text{SSIM}(\boldsymbol{s}, \hat{\boldsymbol{s}}) = \frac{(2\mu_s\mu_{\hat{s}} + \text{C}_1)\left(2\sigma_{s\hat{I}} + \text{C}_2\right)}{\left(\mu_s^2 + \mu_{\hat{s}}^2 + \text{C}_1\right)\left(\sigma_s^2 + \sigma_{\hat{s}}^2 + \text{C}_2\right)}. \tag{9}$$

IV. PROPOSED RGB-TV

Suppose an N × N × 3 pixels of CRI with RGB format, this paper proposes RGB-TV which is consist of CS and reconstruction as shown in Fig. 3. In CS steps as shown in Fig. 3(a), first, an original CRI is represented by an unsigned integer matrices $\boldsymbol{I} \in \mathbb{Z}^{N \times N \times 3}$, then the original CRI is separated to RGB layer $\boldsymbol{I}_l \in \mathbb{R}^{N \times N}$. Second, RGB loops are performed. For each loop, in SS Fourier sampling, $\boldsymbol{I}_l \in \mathbb{Z}^{N \times N}$ image is reshaped to a signal $\boldsymbol{x} \in \mathbb{R}^{n \times 1}$ with $n = N \times N$ as k-sparse input signal and m sample is measured to obtain measured vector where $k < m < n$ as the CS rule or $0 < \frac{m}{n} < 1$. The RGB loops are finished when all R, G, and B layers are sampled. In reconstruction as shown in Fig. 3(b), a compressed image is reconstructed from the measured vector. Then, RGB loops are performed on each measured vector. TV-based reconstruction is performed for each loop to recover the image from the compressed image. Then, check the condition of the end loop. If the loop is a B layer, the process is finished with the result of RGB images, and the reconstructed image is obtained. While, if the loop is not B layer, then continue to the next loop. Algorithm 1 describes the step of reconstruction.

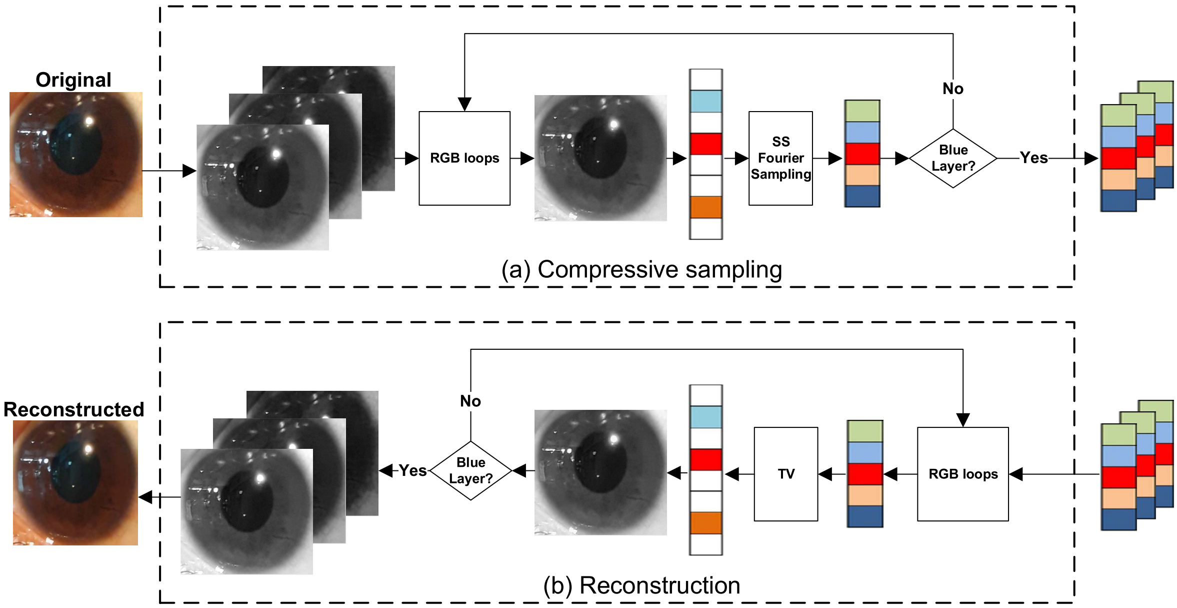

FIGURE 3. The illustration of proposed RGB-TV for CRI compression.

Algorithm 1: RGB-TV

Input: Compressed vector $\boldsymbol{y} \in \mathbb{R}^{m\times 1\times 3}$, sampling matrix $\boldsymbol{\Phi} \in \mathbb{R}^{m\times n}$, and ε
Output: The reconstructed CRI $\hat{\boldsymbol{s}} \in \mathbb{Z}^{N\times N\times 3}$
for $l \leftarrow 1$ **to** 3 **do**
  Initialization $t = 1$;
  while $t < t_{max}$ *and* $\alpha > \varepsilon$ **do**
    Compute the projection onto the L_2-ball $\min_{\hat{x}} \|\boldsymbol{x} - \hat{\boldsymbol{x}}\|_2^2$ s.t. $\|\boldsymbol{y} - \boldsymbol{\Phi}\hat{\boldsymbol{x}}\|_2 \leq \varepsilon$;
    Compute TV norm $\|\hat{\boldsymbol{x}}\|_{\mathrm{TV}}$;
    Compute the TV proximal operator $\min_{\hat{x}} \|\boldsymbol{x} - \hat{\boldsymbol{x}}\|_2^2 + \lambda \|\hat{\boldsymbol{x}}\|_{\mathrm{TV}}$;
    Update $\alpha = \frac{\left\|\hat{\boldsymbol{x}}^{(t)} - \hat{\boldsymbol{x}}^{(t-1)}\right\|_{\mathrm{TV}}}{\left\|\hat{\boldsymbol{x}}^{(t-1)}\right\|_{\mathrm{TV}}}$;
    $t \leftarrow t + 1$;
  end
  $\hat{s}_l = \hat{x}$;
end

A. SSFS

SSFS is a process to sample a CRI to get compressed signal using a masking matrix (denoted as $\mathbf{M}$) and spectrum matrix (denoted as $\mathbf{A}$) in a domain of discrete Fourier transform matrix (denoted as $\mathbf{F}$). The SSFS is a CS using $\boldsymbol{\Phi} = \mathbf{MFA}$, where $\mathbf{M} \in \mathbb{R}^{m\times n}$ is a rectangular binary matrix, $\mathbf{F} \in \mathbb{C}^{n\times n}$ is a complex matrix, and $\mathbf{A} \in \mathbb{R}^{n\times n}$ is a diagonal matrix. In addition, $\mathbf{MFA}$ can be the inverse transformed that considers $\mathbf{1}_M \in \mathbb{R}^M$ and defined as

$$\mathbf{F}^{\mathrm{T}}\mathbf{M}^{\mathrm{T}}\mathbf{1}_M, \tag{10}$$

In SSFS [38], a noise with input signal-to-noise ratio (ISNR) is considered and the CS process becomes

$$\boldsymbol{y} = \boldsymbol{\Phi}\boldsymbol{x} + \boldsymbol{w}, \tag{11}$$

where $\boldsymbol{w}$ represents the noise and the ISNR is determined as

$$\mathrm{ISNR} = 10\log_{10}\left(\frac{\|\boldsymbol{\Phi}\boldsymbol{x}\|_2}{\|\boldsymbol{w}\|_2}\right)^2. \tag{12}$$

B. TV RECONSTRUCTION

In reconstruction process, to reconstruct $\boldsymbol{x}$ according to $\boldsymbol{\Phi}$, the problem of TV proximal operator [39] is defined as

$$\min_{\hat{x}} \|\boldsymbol{x} - \hat{\boldsymbol{x}}\|_2^2 + \lambda \|\hat{\boldsymbol{x}}\|_{\mathrm{TV}}, \tag{13}$$

where $\hat{\boldsymbol{x}}$ is a reconstructed signal from the TV.

V. EXPERIMENT

This section presents the experiment to investigate the performance of the proposed RGB-TV. First, retinal images are presented. Second, the experiment scenario is presented. Last, hardware and software specifications are elaborated.

A. CRI

In this paper, real CRI data is considered from a patient at TelkomMedika hospital, Bandung, Indonesia. The acquisition was acquired by one expert operator from the high cholesterol patients. The CRI data consists of 90 images with *.bmp format, RGB colored channel, 660 × 603 pixels, and 8-bit pixel depth. Furthermore, to make a fair comparison of different CMI methods, $N \times N$ with $N = 64, 128, 256, 512$ are investigated in this paper.

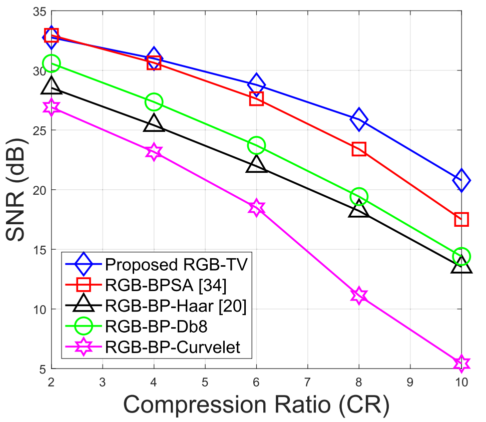

FIGURE 4. The effect of CR to SNR.

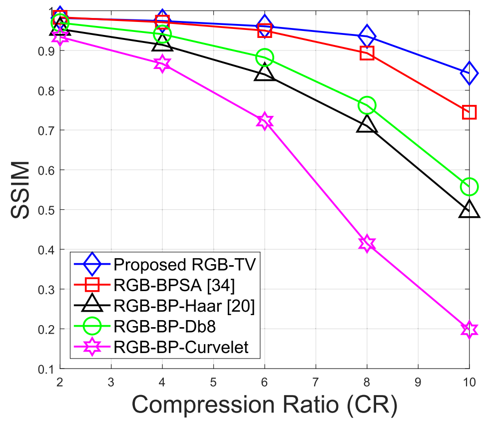

FIGURE 5. The effect of CR to SSIM.

B. EXPERIMENT SCENARIO

This section presents the experiment scenario, first, an $N \times N$ pixels of CRI is considered as the original image. Second, CS is performed according to CR for CRI compression to get a compressed vector. Third, reconstruction is performed by using RGB-TV as presented in Algorithm 1 to recover the reconstructed image from a compressed vector. Last, performance metrics are calculated to investigate the original and reconstructed CRI. Furthermore, the effect of parameters are presented as follows

- Performance metrics with regards to CR, where $N = 64$ is considered as fixed resolution and the different CRs are investigated.
- Performance metrics with regards to ISNR, where $N = 64$ is considered as fixed resolution, CR $= 0.5$ is considered, and ISNR is investigated.
- Performance metrics with regards to N, where 128×128, 256×256, and 512×512 pixels are investigated.

This paper compares RGB-TV, RGB-BPSA [34], RGB BP with state-of-the-arts with Haar basis [20], Daubechies 8 (Db8) basis, and curvelet basis. The RGB-TV for CRI is implemented using MATLAB R2020b in a personal computer with a processor 3.20GHz Intel(R) Core(TM) i-8700 CPU and 16GB memory. These specifications are required to validate the processing time results to make a fair comparison with other CMI methods.

VI. EXPERIMENT RESULTS

This section presents the experimental results to validate the scenario and performance metrics presented in Section V-B. The comparison of proposed RGB-TV, RGB-BPSA [34], RGB-BP with state-of-the-arts with Haar basis [20], Daubechies 8 (Db8) basis, and curvelet basis are presented.

A. COMPRESSION RATIO (CR)

Fig. 4 shows the effect of CR to SNR results of proposed RGB-TV, RGB-BPSA [34], RGB-BP-Haar [20], RGB-BP-Db8, and RGB-BP-Curvelet. X and Y-value refer to CR $= 2, 4, 6, 8, 10$ and SNR in dB, respectively. The results show that the proposed RGB-TV outperforms all CS benchmarks. Targeting SNR $>$ 20 dB, RGB-TV achieves at all CR conditions while RGB-BPSA achieves CR $\leq$ 9. In addition, the result of RGB-TV and RGB-BPSA at CR $=$ 2 are obtained as similar SNR results, then detailed results of SNR are presented in Table 1 and Fig. 6. The boxplot results of SNR with CR $=$ 2, 4, and 6 are shown in Fig. 6(a), (b), and (c), respectively. The SNR results in boxplot graphs show that the proposed RGB-TV outperforms all CMIs at CR $=$ 4 and 6 with the highest median value of SNR as shown in solid red lines. The median value of RGB-TV at CR $=$ 2 is lower than RGB-BPSA but the minimum value of RGB-TV is higher than RGB-BPSA. From Fig. 6, it is validated that RGB-TV outperforms RGB-BPSA at higher CR and more convergence than RGB-BPSA. The same trends are also presented in Table 1 where the mean SNR of the proposed RGB-TV is the best result at all CR conditions.

Next, Fig. 5 shows the results to investigate the SSIM of RGB-TV with regards to CR $= 2, 4, 6, 8, 10$. X-value corresponds to CR and Y-value corresponds to SSIM. The results show that the proposed RGB-TV outperforms all benchmark CMIs. Suppose to aim SSIM$>$ 0.8, the proposed RGBV-TV achieves at CR $\leq$ 10 while RGB-BPSA achieves at CR $\leq$ 9. A detailed results of SSIM at CR $\leq$ 6 are presented in Table 2 and Fig. 7 to show the difference of the proposed and BPSA results at CR $\leq$ 6. The boxplot results os SSIM with CR $=$ 2, 4, and 6 are shown in Fig. 7(a), (b), and (c), respectively. The SSIM results in boxplot graphs show that the proposed RGB-TV outperforms all CMIs at CR $=$ 4 and 6 with the highest median value of SSIM as shown in solid red lines. The median value of RGB-TV at CR $=$ 2 is lower than RGB-BPSA but the maximum value of RGB-TV is higher than RGB-BPSA. From Fig. 7, it is validated that RGB-TV achieved better visual than RGB-BPSA at higher CR and more convergence than RGB-BPSA. In addition, Table 1 shows that the proposed RGB-TV is the best SSIM results

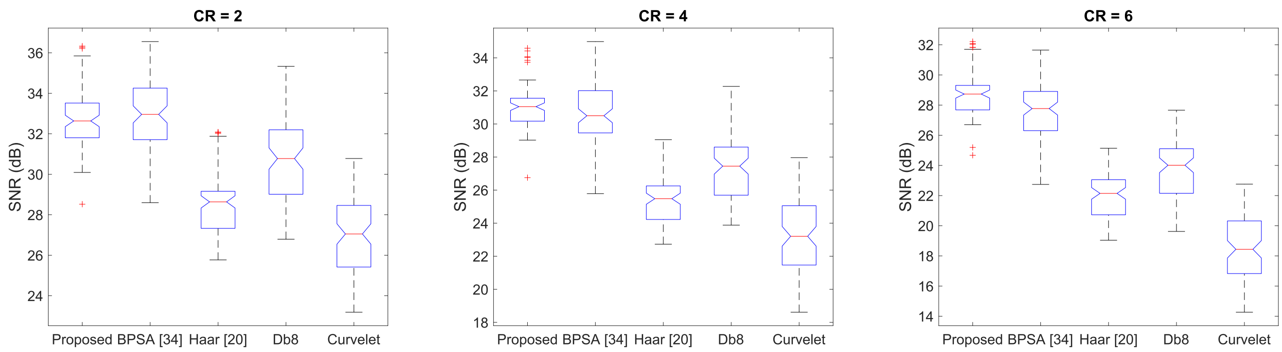

(a) (b) (c)

FIGURE 6. Boxplot of ASNR results at CR $\leq$ 6.

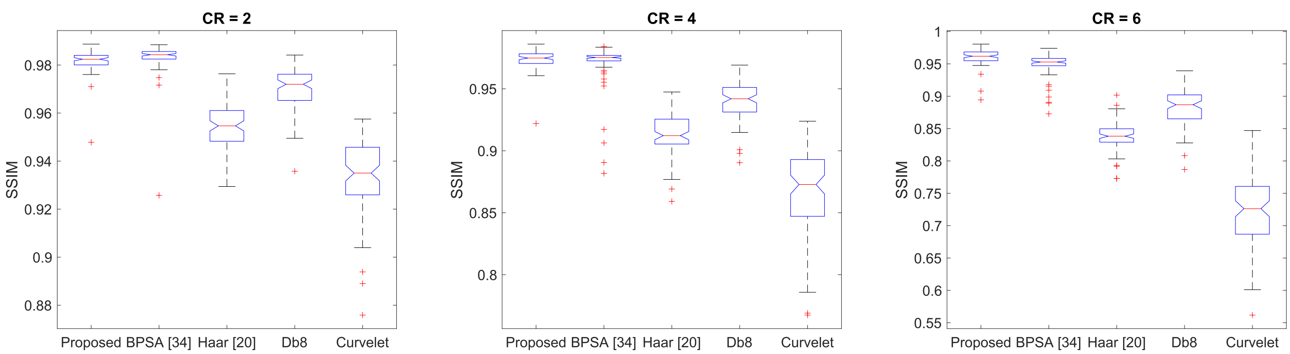

(a) (b) (c)

FIGURE 7. Boxplot of SSIM results at CR $\leq$ 6 for proposed and BPSA.

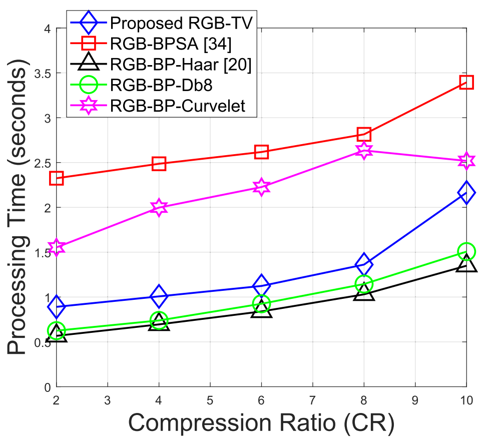

FIGURE 8. The effect of CR to processing time.

at CR $>$ 4 with a higher mean SSIM and lower standard deviation.

Last, Fig. 8 shows processing results to analyze the performance of the proposed RGB-TV, RGB-BPSA, RGB-BP-Haar, RGB-BP-DB8, and RGB-BP-Curvelet. The fastest processing time result is RGB-BP-Haar but

TABLE 1. Mean and standard deviation of Fig. 4 at CR $\leq$ 6.

	CR = 2	CR = 4	CR = 6
Proposed	32.75 ± 0.40	30.99 ± 0.27	28.78 ± 0.33
BPSA	32.93 ± 0.34	30.63 ± 0.39	27.62 ± 0.12
Haar	28.53 ± 0.12	25.39 ± 0.10	21.96 ± 0.16
Db8	30.58 ± 0.13	27.34 ± 0.12	23.70 ± 0.07
Curvelet	26.90 ± 0.08	23.16 ± 0.07	18.48 ± 0.06

RGB-BP-Haar obtains the second worts SNR and SSIM results. The longest processing time is RGB-BPSA which is achieved $\sim$ 3.4 seconds at CR = 10. The processing time of RGB-TV is half times of RGB-BPSA and it is validated that RGB-TV outperforms all CMIs in the view of SNR, SSIM, and processing time.

B. EFFECT OF ISNR

The effect of ISNR on SNR results is shown in Fig. 9(a). Targeting SNR $\geq$ 30 dB, both RGB-TV and RGB-BPSA are achieved at ISNR $\geq$ 23 dB. It is shown that RGB-TV and RGB-BPSA are obtained similar SNR results, then detailed results of SNR are presented in Fig. 10. The boxplot results of SNR at ISNR = 10, 30, and 50 dB are shown in Fig. 10(a), (b), and (c), respectively. For all ISNR conditions, the proposed

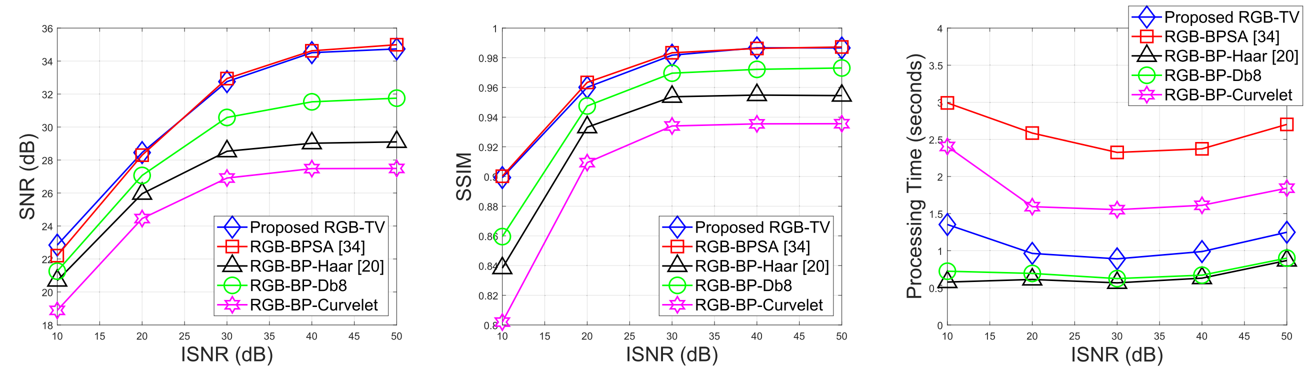

(a) (b) (c)

FIGURE 9. Effect of ISNR to performance metrics.

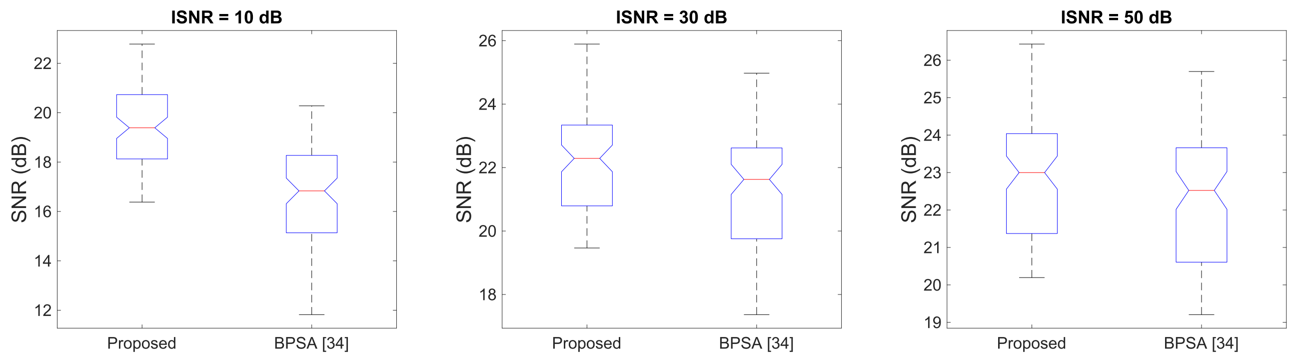

(a) (b) (c)

FIGURE 10. Boxplot of ASNR results at ISNR = 10, 30, 50 for proposed and BPSA.

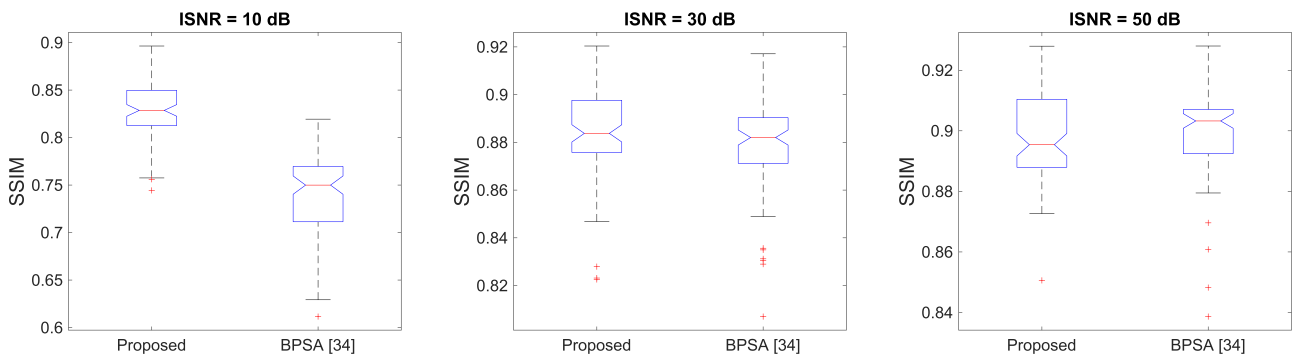

(a) (b) (c)

FIGURE 11. Boxplot of SSIM results at ISNR = 10, 30, 50 for proposed and BPSA.

RGB-TV outperforms RGB-BPSA with higher median, minimum, and maximum values in the boxplot results.

The effect of ISNR on SSIM results is shown in Fig. 9(b). Targeting SSIM $\geq$ 0.98 dB, both RGB-TV and RGB-BPSA are achieved at ISNR $\geq$ 30. The SSIM of RGB-TV and RGB-BPSA are converged around 0.98 at ISNR $\geq$ 40. The SSIM of RGB-BP-Db8 is converged around 0.97 at ISNR $\geq$ 30 dB. The SSIM of RGB-BP-Haar is converged around 0.958 at ISNR $\geq$ 30 dB, and the SSIM of RGB-BP-Curvelet is converged around 0.937 at ISNR $\geq$ 30 dB. It is shown that RGB-TV and RGB-BPSA are obtained similar SSIM results, then detailed results of SSIM are presented in Fig. 11. The boxplot results are presented to show the detailed SSIM results of RGB-TV and RGB-BPSA. The results show

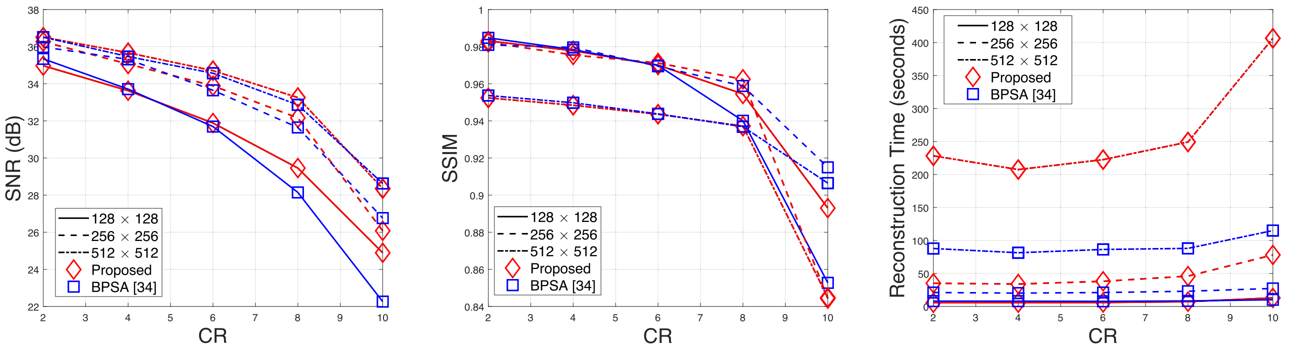

(a) (b) (c)

FIGURE 12. Effect of resolutions to performance metrics.

TABLE 2. Mean and standard deviation of Fig. 5 at CR ≤ 6.

	CR = 2	CR = 4	CR = 6
Proposed	0.981 ± 0.005	0.974 ± 0.007	0.960 ± 0.011
BPSA	0.983 ± 0.008	0.971 ± 0.017	0.950 ± 0.004
Haar	0.953 ± 0.001	0.914 ± 0.002	0.839 ± 0.003
Db8	0.969 ± 0.003	0.941 ± 0.003	0.882 ± 0.003
Curvelet	0.934 ± 0.001	0.866 ± 0.005	0.722 ± 0.004

TABLE 3. The detailed SSIM results of Fig. 9.

ISNR	SNR (dB)		SSIM	
	Proposed	BPSA	Proposed	BPSA
10	22.84 ± 0.09	28.45 ± 0.11	0.910 ± 0.001	0.960 ± 0.002
20	22.20 ± 0.09	28.29 ± 0.15	0.900 ± 0.005	0.963 ± 0.006
30	20.68 ± 0.08	25.95 ± 0.11	0.838 ± 0.001	0.933 ± 0.001
40	21.25 ± 0.09	27.06 ± 0.14	0.859 ± 0.000	0.947 ± 0.000
50	18.88 ± 0.35	24.45 ± 0.22	0.801 ± 0.037	0.909 ± 0.019

that the median value of RGB-TV outperforms RGB-BPSA at ISNR = 10 dB, while RGB-BPSA outperforms RGB-TV at ISNR = 30 and 50 dB. The maximum value of RGB-TV outperforms RGB-BPSA at all ISNR conditions and it is validated that the visual quality result of RGB-TV outperforms RGB-BPSA.

In addition, Table 3 presents the mean and standard deviation results of SSIM concerning ISNR. The results show that RGB-TV outperforms RGB-BPSA at all ISNR conditions with higher mean and lower standard deviation.

Last, Fig. 9(c) shows processing results to analyze the performance of RGB-TV. At all ISNR conditions, RGB-TV and RGB-BPSA are compared, where RGB-TV outperforms RGB-BPSA with less processing time.

C. THE EFFECT OF RESOLUTIONS

Fig. 12(a) shows the effect of resolutions to ASNR. The highest ASNR = 42.53 dB is achieved by 256 × 256 at CR = 2 while the lowest ASNR = 24.96 dB is achieved by 64 × 64 at CR = 10. Aiming ASNR > 30 dB, 64 × 64 attains ASNR ≥ 31.40 dB at CR ≤ 8, ASNR ≥ 32.22 dB is achieved by 128 × 128 at CR ≤ 10, and 256 × 256 attains ASNR ≥ 37.24 dB at CR ≤ 10.

Fig. 12(b) shows the effect of resolutions to SSIM. The highest SSIM = 0.9941 is achieved by 245 × 256 at CR = 2 while the lowest SSIM = 0.8961 is achieved by 64 × 64 at CR = 10. Aiming SSIM > 0.950, 64 × 64 attains SSIM ≥ 0.9612 at CR ≤ 8, SSIM ≥ 0.9612 is attained by 128×128 at CR ≤ 10, and 256×256 attains SSIM ≥ 0.9846 at CR ≤ 10.

Fig. 12(c) shows the effect of resolutions to processing time results. The fastest processing time = 4.04 seconds is achieved by 64 × 64 at CR = 10 while the longest processing time = 44.33 seconds is achieved by 128 × 128 at CR = 8.

VII. CONCLUSION

This paper proposed a CS framework for compression of a color retinal image using spread spectrum (SS) Fourier sampling and three loops of RGB layers based on TV reconstruction. The proposed CS is referred to as RGB-TV and compared to the recent RGB-BPSA [34]. RGB-TV outperforms the state-the-arts CS using BP (i.e., curvelet, haar, and db8 sparsity basis) and RGB-BPSA. Computer simulation results demonstrated that the proposed RGB-TV achieved better visual quality and faster processing time for CS reconstruction of CRI with a resolution of 64 × 64 pixels.

For future works, sparse Bayesian learning (SBL) [40] can be considered as a new framework for CMI and an investigation of efficient multitask structure-aware SBL to color retinal images.

REFERENCES

[1] Y. Zhou, G. Li, and H. Li, "Automatic cataract classification using deep neural network with discrete state transition," *IEEE Trans. Med. Imag.*, vol. 39, no. 2, pp. 436–446, Feb. 2020.

[2] M. Z. Atwany, A. H. Sahyoun, and M. Yaqub, "Deep learning techniques for diabetic retinopathy classification: A survey," *IEEE Access*, vol. 10, pp. 28642–28655, 2022.

[3] S. N. Andana, L. Novamizanti, and I. N. A. Ramatryana, "Measurement of cholesterol conditions of eye image using fuzzy local binary pattern (FLBP) and linear regression," in *Proc. IEEE Int. Conf. Signals Syst. (ICSigSys)*, Jul. 2019, pp. 79–84.

[4] C. A. Nurbani, L. Novamizanti, I. N. A. N. Ramatryana, and N. P. D. P. Wardana, "Measurement of cholesterol levels through eye based on co-occurrence matrix on android," in *Proc. IEEE Asia Pacific Conf. Wireless Mobile (APWiMob)*, Nov. 2019, pp. 88–93.

[5] J. Raharjo, L. Novamizanti, and I. N. A. Ramatryana, "Cholesterol level measurement through iris image using gray level co-occurrence matrix and linear regression," *ARPN J. Eng. Appl. Sci.*, vol. 14, no. 21, p. 1, 2019.
[6] Y. Yuan, L. Zhang, L. Wang, and H. Huang, "Multi-level attention network for retinal vessel segmentation," *IEEE J. Biomed. Health Informat.*, vol. 26, no. 1, pp. 312–323, Jan. 2022.
[7] C. Baek and J.-M. Seo, "Encapsulation material for retinal prosthesis with photodetectors or photovoltaics," *IEEE Sensors J.*, vol. 22, no. 2, pp. 1767–1774, Jan. 2022.
[8] T. W. Cabral, M. Khosravy, F. M. Dias, H. L. M. Monteiro, M. A. A. Lima, L. R. M. Silva, R. Naji, and C. A. Duque, "Compressive sensing in medical signal processing and imaging systems," in *Sensors for Health Monitoring*. Amsterdam, The Netherlands: Elsevier, 2019, pp. 69–92.
[9] L. Shen and R. M. Rangayyan, "A segmentation-based lossless image coding method for high-resolution medical image compression," *IEEE Trans. Med. Imag.*, vol. 16, no. 3, pp. 301–307, Jun. 1997.
[10] A. Munteanu, J. Cornelis, and P. Cristea, "Wavelet-based lossless compression of coronary angiographic images," *IEEE Trans. Med. Imag.*, vol. 18, no. 3, pp. 272–281, Mar. 1999.
[11] Z.-D. Chen, R.-F. Chang, and W.-J. Kuo, "Adaptive predictive multiplicative autoregressive model for medical image compression," *IEEE Trans. Med. Imag.*, vol. 18, no. 2, pp. 181–184, Feb. 1999.
[12] V. Sanchez, P. Nasiopoulos, and R. Abugharbieh, "Efficient lossless compression of 4-D medical images based on the advanced video coding scheme," *IEEE Trans. Inf. Technol. Biomed.*, vol. 12, no. 4, pp. 442–446, Jul. 2008.
[13] V. Sanchez, R. Abugharbieh, and P. Nasiopoulos, "Symmetry-based scalable lossless compression of 3D medical image data," *IEEE Trans. Med. Imag.*, vol. 28, no. 7, pp. 1062–1072, Jul. 2009.
[14] L. F. R. Lucas, N. M. M. Rodrigues, L. A. da Silva Cruz, and S. M. M. de Faria, "Lossless compression of medical images using 3-D predictors," *IEEE Trans. Med. Imag.*, vol. 36, no. 11, pp. 2250–2260, Nov. 2017.
[15] Z. Chen, S. Gu, G. Lu, and D. Xu, "Exploiting intra-slice and inter-slice redundancy for learning-based lossless volumetric image compression," *IEEE Trans. Image Process.*, vol. 31, pp. 1697–1707, 2022.
[16] S.-G. Miaou and S.-T. Chen, "Automatic quality control for wavelet-based compression of volumetric medical images using distortion-constrained adaptive vector quantization," *IEEE Trans. Med. Imag.*, vol. 23, no. 11, pp. 1417–1429, Nov. 2004.
[17] V. Sanchez, R. Abugharbieh, and P. Nasiopoulos, "3-D scalable medical image compression with optimized volume of interest coding," *IEEE Trans. Med. Imag.*, vol. 29, no. 10, pp. 1808–1820, Oct. 2010.
[18] S. Parikh, D. Ruiz, H. Kalva, G. Fernández-Escribano, and V. Adzic, "High bit-depth medical image compression with HEVC," *IEEE J. Biomed. Health Inform.*, vol. 22, no. 2, pp. 552–560, Mar. 2018.
[19] D. Rossinelli, G. Fourestey, F. Schmidt, B. Busse, and V. Kurtcuoglu, "High-throughput lossy-to-lossless 3D image compression," *IEEE Trans. Med. Imag.*, vol. 40, no. 2, pp. 607–620, Feb. 2021.
[20] D. L. Donoho, "Compressed sensing," *IEEE Trans. Inf. Theory*, vol. 52, no. 4, pp. 1289–1306, Apr. 2016.
[21] E. J. Candès and M. B. Wakin, "An introduction to compressive sampling," *IEEE Signal Process. Mag.*, vol. 25, no. 2, pp. 21–30, Mar. 2008.
[22] L. Wang, L. Li, L. Jin, L. Jing, B. B. Gupta, and L. Xia, "Compressive sensing of medical images with confidentially homomorphic aggregations," *IEEE Internet Things J.*, vol. 6, no. 2, pp. 1402–1409, Apr. 2019.
[23] F. Gan, C. Luo, H. Wang, and B. Deng, "Robust compressive terahertz coded aperture imaging using deep priors," *IEEE Geosci. Remote Sens. Lett.*, vol. 19, pp. 1–5, 2022.
[24] M. Liang, Y. Li, H. Meng, M. A. Neifeld, and H. Xin, "Reconfigurable array design to realize principal component analysis (PCA)-based microwave compressive sensing imaging system," *IEEE Antennas Wireless Propag. Lett.*, vol. 14, pp. 1039–1042, 2015.
[25] S. Zhou, Z. Luo, N. Xiu, and G. Y. Li, "Computing one-bit compressive sensing via double-sparsity constrained optimization," *IEEE Trans. Signal Process.*, vol. 70, pp. 1593–1608, 2022.
[26] J. Wang, W. Su, C. Luo, J. Chen, H. Song, and J. Li, "CSG: Classifier-aware defense strategy based on compressive sensing and generative networks for visual recognition in autonomous vehicle systems," *IEEE Trans. Intell. Transp. Syst.*, early access, Feb. 14, 2022, doi: 10.1109/TITS.2022.3146038.
[27] H. Wang, J. Fang, H. Duan, and H. Li, "Compressive wideband spectrum sensing and signal recovery with unknown multipath channels," *IEEE Trans. Wireless Commun.*, early access, Jan. 7, 2022, doi: 10.1109/TWC.2021.3139294.
[28] L. R. Shiddik, L. Novamizanti, I. N. A. N. Ramatryana, and H. A. Hanifan, "Compressive sampling for robust video watermarking based on BCH code in SWT-SVD domain," in *Proc. Int. Conf. Sustain. Eng. Creative Comput. (ICSECC)*, Aug. 2019, pp. 223–227.
[29] M. D. Godole, L. Novamizanti, and I. N. A. Ramatryana, "RS code and compressive sampling on video watermarking-based DWT-SVD," in *Proc. 4th Int. Conf. Inf. Technol., Inf. Syst. Electr. Eng. (ICITISEE)*, Nov. 2019, pp. 541–546.
[30] M. Jacob, J. C. Ye, L. Ying, and M. Doneva, "Computational MRI: Compressive sensing and beyond [from the guest editors]," *IEEE Signal Process. Mag.*, vol. 37, no. 1, pp. 21–23, Jan. 2020.
[31] T. Rahim, L. Novamizanti, I. N. Apraz Ramatryana, and S. Y. Shin, "Compressed medical imaging based on average sparsity model and reweighted analysis of multiple basis pursuit," *Comput. Med. Imag. Graph.*, vol. 90, Jun. 2021, Art. no. 101927.
[32] X. Zeng, S. Tong, Y. Lu, L. Xu, and Z. Huang, "Adaptive medical image deep color perception algorithm," *IEEE Access*, vol. 8, pp. 56559–56571, 2020.
[33] R. Magdalena, T. Rahim, I. P. A. E. Pratama, L. Novamizanti, I. N. A. Ramatryana, A. Y. Raja, and S. Y. Shin, "RGB-based compressed medical imaging using sparsity averaging reweighted analysis for wireless capsule endoscopy images," *IEEE Access*, vol. 9, pp. 147091–147101, 2021.
[34] T. Rahim, R. Magdalena, I. P. A. E. Pratama, L. Novamizanti, I. N. A. Ramatryana, S. Y. Shin, and D. S. Kim, "Basis pursuit with sparsity averaging for compressive sampling of iris images," *IEEE Access*, vol. 10, pp. 13728–13737, 2022.
[35] R. E. Carrillo, J. D. McEwen, and Y. Wiaux, "Sparsity averaging reweighted analysis (SARA): A novel algorithm for radio-interferometric imaging," *Mon. Not. Roy. Astron. Soc.*, vol. 426, no. 2, pp. 1223–1234, 2012.
[36] I. N. A. Ramatryana, T. Rahim, and S. Y. Shin, "Compressed medical imaging using doubly Parseval frame sparsity averaging," in *Proc. Summer Comprehensive Conf.*, 2020, pp. 206–207.
[37] T. Rahim, L. Novamizanti, I. N. A. Ramatryana, S. Y. Shin, and D. S. Kim, "Total variant based average sparsity model with reweighted analysis for compressive sensing of computed tomography," *IEEE Access*, vol. 9, pp. 119158–119170, 2021.
[38] G. Puy, P. Vandergheynst, R. Gribonval, and Y. Wiaux, "Universal and efficient compressed sensing by spread spectrum and application to realistic Fourier imaging techniques," *EURASIP J. Adv. Signal Process.*, vol. 2012, no. 1, pp. 1–13, Dec. 2012.
[39] E. J. Candès, Y. C. Eldar, D. Needell, and P. Randall, "Compressed sensing with coherent and redundant dictionaries," *Appl. Comput. Harmon. Anal.*, vol. 31, no. 1, pp. 59–73, Jul. 2011. [Online]. Available: https://www.sciencedirect.com/science/article/pii/S1063520310001156
[40] S. Liu, Y. Huang, H. Wu, C. Tan, and J. Jia, "Efficient multitask structure-aware sparse Bayesian learning for frequency-difference electrical impedance tomography," *IEEE Trans. Ind. Informat.*, vol. 17, no. 1, pp. 463–472, Jan. 2021.

LEDYA NOVAMIZANTI (Student Member, IEEE) received the bachelor's degree in mathematics from Andalas University, in 2005, and the master's degree in electrical and telecommunication engineering from Telkom University, in 2008. She is currently pursuing the Ph.D. degree with Institut Teknologi Bandung. Since 2010, she has been working as a Lecturer with Telkom University. Her current research interests include image processing, data hiding, and machine learning.

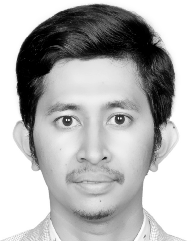

I NYOMAN APRAZ RAMATRYANA (Student Member, IEEE) received the bachelor's degree in telecommunication engineering from the Telkom Institute of Technology (currently known as Telkom University), Indonesia, in 2010, and the master's degree in electrical and telecommunication engineering from Telkom University, Indonesia, in 2014. He is currently pursuing the Ph.D. degree in IT convergence engineering with the Kumoh National Institute of Technology, South Korea. His areas of expertise are signal processing, artificial intelligence (AI), wireless communications, and computer vision. His research interests include random access (RA), raptor coding, non-orthogonal multiple access (NOMA), multiple-input multiple-output (MIMO) antenna, compressed imaging, and medical imaging, deep learning (DL).

RITA MAGDALENA received the Bachelor of Engineering degree in electrical engineering from North Sumatera University, Indonesia, in 1987, and the Master of Engineering degree in electrical engineering from the Bandung Institute of Technology, Indonesia, in 2001. She has been working as a Lecturer with Telkom University, since 1999. Her current research interests include signal processing and artificial intelligence.

I PUTU AGUS EKA PRATAMA received the bachelor's degree in informatics from the Institut Teknologi Telkom, and the master's degree in informatics from the Institut Teknologi Bandung (ITB). He has been working as a Researcher and a Lecturer with the Information Network and System (INS) Research Laboratory, ITB. Since 2015, he has been as a Lecturer with the Department of Information Technology, Faculty of Engineering, Udayana University. His research interests include smart city, big data, computer networks, computer security, Linux, and intelligent transportation systems. He has been an ICT Consultant and the author of 12 ICT books, since 2014.

TARIQ RAHIM (Member, IEEE) received the Ph.D. degree majoring in IT convergence engineering from the WENS Laboratory, Kumoh National Institute of Technology (KIT), South Korea, in 2021. Previously, he was working as a Postdoctoral Fellow and a Researcher with the ICT-CRC, KIT, South Korea. He is currently working as a Postdoctoral Research Fellow with the School of Cardiff School of Health and Sciences, Cardiff Metropolitan University, U.K. His research interests include image processing, medical image analysis, deep learning, video processing, and quality of services of high frame rate videos.

SOO YOUNG SHIN (Senior Member, IEEE) received the B.S., M.S., and Ph.D. degrees in electrical engineering and computer science from Seoul National University, South Korea, in 1999, 2001, and 2006, respectively. He was a Visiting Scholar with the FUN Laboratory, University of Washington, USA, from July 2006 to June 2007. After three years working with the WiMAX design Laboratory, Samsung Electronics. He has been an Associate Professor with the School of Electronics, Kumoh National Institute of Technology, since September 2010. His research interests include wireless LAN, WPAN, WBAN, wireless mesh networks, sensor networks, coexistence among wireless networks, industrial and military networks, cognitive radio networks, and next generation mobile wireless broadband networks.